

# Solution of Two-Dimensional Viscous Flow Driven by Motion of Flexible Walls

Ravi Bhadauria, Ramana M. Pidaparti and Mohamed Gad-el-Hak

<sup>a</sup> Department of Mechanical Engineering, Virginia Commonwealth University  
Richmond, VA 23284, U.S.A.

Received: 16/11/2009 – Revised 02/03/2010 – Accepted 09/03/2010

## Abstract

An exact solution of the Navier–Stokes equations for a flow driven by motion of a flexible wall is developed. A simple two-dimensional channel with deforming walls is considered as the domain. The governing equations are linearized for low Reynolds and large Womersley number Newtonian flows. Appropriate boundary conditions for general deformation are decomposed into harmonic excitations in space by Fourier series decomposition. A model of harmonic boundary deformation is considered and the results are compared with computational fluid dynamics predictions. The results of velocity profiles across the channel and the centerline of the channel are in good agreement with CFD solution. The analytical model developed provides quantitative descriptions of the flow field for a wide spectrum of actuating frequency and boundary conditions. The presented model can be used as an effective framework for preliminary design and optimization of displacement micropumps and other miniature applications.

**Keywords:** *Micropumps; Viscous flow; Computational fluid dynamics; Flexible wall; Boundary driven flow; Upper/lower wall deformation.*

## 1. Introduction

There has been a tremendous interest in understanding the nature of flow in biological systems, such as flow in arteries [1, 2] and alternative pumping techniques for microfluidic flow requirements which are of the order of 1 cm<sup>3</sup> or less [3–5]. Efforts have been made on both theoretical [1, 2, 6–8] and numerical [9–11] fronts to investigate the complicated physics behind pulsatile pumping which is important in pulmonary flows and displacement micropumps. In particular, peristaltic pumps, in which the motion of the fluid resembles the periodic motion of the esophagus, is of significant importance.

There have been extensive theoretical studies performed on peristaltic pumping which incorporates sinusoidal, infinitely long, two dimensional, and continuous models, for both small amplitudes and long wavelength peristaltic waves [7, 8, 12]. In earlier works, there is reference to some unique features of peristaltic flow, such as ‘reflux’ and ‘trapping’ in comparison to biological flows [8]. Reflux happens when the mean retrograde velocity of the fluid is opposite to the direction of wave propagation, while trapping occurs because of stationary recirculation and the fluid is unable to move within the mainstream [12]. Researchers have investigated modeling peristaltic motion for infinitely long geometries with long amplitudes and low Reynolds numbers, using asymptotic methods [6]. Also some studies have performed analysis on finite length tubes with continuous waves [13], but almost negligible efforts have been made to study flows in a finite

channel where walls are fixed at the ends. There have been some efforts to perform simulation on peristaltic pumps with fixed ends that are arranged in a cascade [14]. Also, the flows in these devices are driven by pulsating pressure where the deformation is subject to the pressure gradient imposed. Based on the literature, it appears that there is a need to develop a mathematical framework that is useful for providing a theoretical perspective of moving boundary driven flows.

The current study was motivated when the authors were developing a novel design for a MEMS device and optimizing it for targeting a particular flow rate [15, 16]. The device is a peristaltic action micropump, consisting of four pneumatically actuated nozzle/diffuser shaped moving actuators on the sidewalls. These actuators were used to create pressure difference in the four pump chambers, which in turn drove the fluid through the pump in one direction. Due to the uniqueness of the design, it was hard to validate the codes used for numerical study. Therefore, a simple design representing all the essential elements and described by the same physics was considered to represent analytical validation, which led to the motivation for the present study.

In this paper, we address the need for providing a mathematical model of high viscosity flow in a 2-D channel, driven by deformation of the surrounding walls. We start with the linearization and decoupling of fundamental equations of motion for an incompressible, Newtonian fluid and seek closure in the system by appropriate no-slip and deformation boundary conditions. We further validate the results obtained from the theoretical model with a CFD solution.

## 2. Analytical approach

### 2.1. Problem definition

We seek an exact solution of Stokes flow between two deforming boundaries in a 2-D channel of length  $L$  as shown in Figure 1. The spatial variation of deformation is a function of the length  $x$  which can be described by a pseudo-periodic function as

$$\bar{\delta}(x,t) = f(x) \sin \omega t \quad (1)$$

where  $f(x)$  can be decomposed into Fourier series which sums up all the modes of vibration as explained in [17] as

$$f(x) = \sum_{n=1}^{\infty} a_n \sin \frac{n\pi}{L} x \quad (2a)$$

$$a_n = \int_0^L f(x) \sin \frac{n\pi x}{L} dx \quad (2b)$$

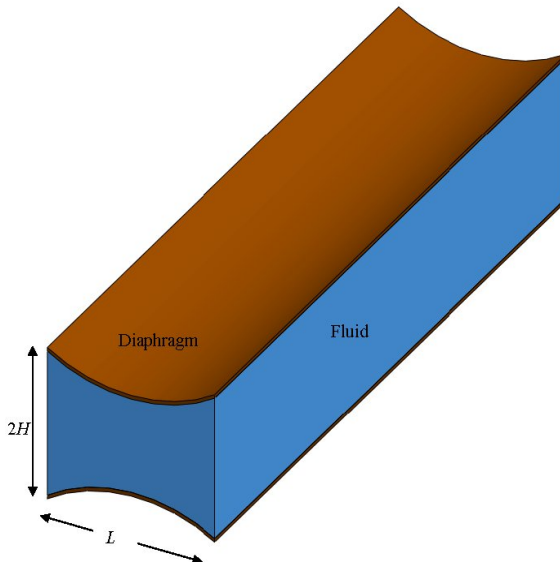


Figure 1. Schematic of model. Drawing not to scale.

In general, one can find the solution for harmonic deformation and sum all the modes to get the total solution. In this study, a solution for fundamental mode of vibration of the wall is presented. The fluid is assumed to be Newtonian, the flow is assumed to be isothermal and having a low Reynolds number, and unsteady in nature. The geometry is presented in Figure 2. The length of the channel is  $L$  and the diameter is  $2H$ , and the displacement at the walls  $y = \pm H$  is given by

$$\delta(x, t) = \pm A \sin kx \sin \omega t \quad (3)$$

where  $A$  is the amplitude of displacement,  $k = \pi/L$  is the wave number, and  $\omega$  is the forcing frequency. The wall deformation can be decomposed into linear superposition of two transverse waves traveling in  $\pm x$  direction as

$$\delta(x, t) = \pm \frac{A}{2} \Re [e^{j(kx - \omega t)} - e^{j(kx + \omega t)}] \quad (4)$$

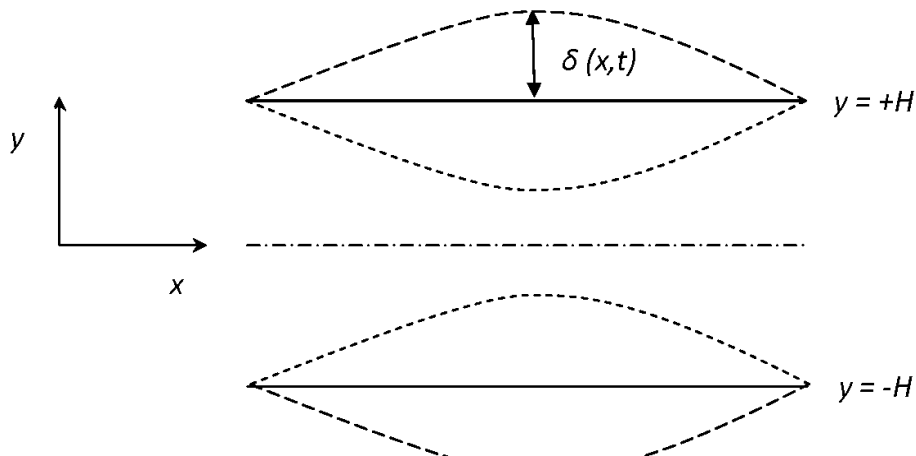


Figure 2. Geometry of model. Drawing not to scale.

### 3. Governing Equations

#### 3.1. Governing equations

Flow is described by set of fluid continuity and momentum conservation equations. Since the flow is highly viscous and laminar, we neglect the convective terms from the Navier–Stokes equations and write the equations for incompressible Newtonian, unsteady, laminar, highly viscous and isothermal flow represented as

$$\frac{\partial u}{\partial x} + \frac{\partial v}{\partial y} = 0 \quad (5a)$$

$$\rho \frac{\partial u}{\partial t} = -\frac{\partial p}{\partial x} + \mu \left[ \frac{\partial^2 u}{\partial x^2} + \frac{\partial^2 u}{\partial y^2} \right] \quad (5b)$$

$$\rho \frac{\partial v}{\partial t} = -\frac{\partial p}{\partial y} + \mu \left[ \frac{\partial^2 v}{\partial x^2} + \frac{\partial^2 v}{\partial y^2} \right] \quad (5c)$$

On comparing the order of terms in the above equations [18]; and by limiting the analysis to disturbances of long wavelengths and large Womersley number ( $\gg 10$ ); and by neglecting terms in  $y$ -momentum equation, we deduce that

$$-\frac{\partial p}{\partial y} = 0 \quad (6a)$$

$$\frac{\partial^2 u}{\partial x^2} \square \frac{\partial^2 u}{\partial y^2} \quad (6b)$$

so  $x$ -momentum equation reduces to

$$\rho \frac{\partial u}{\partial t} = -\frac{\partial p}{\partial x} + \mu \frac{\partial^2 u}{\partial y^2} \quad (7)$$

At this point, it is reasonable to choose the following form of the pressure

$$p(x, t) = p_o + \Re \left[ \hat{p}_1 e^{j(kx - \omega t)} - \hat{p}_2 e^{j(kx + \omega t)} \right] \quad (8)$$

The kernel of exponential  $e^{j(kx \mp \omega t)}$  represents a longitudinal pressure wave traveling in  $\pm x$  direction respectively. Subtracting them, we get a standing wave in pressure where the end value is  $p_o$ . Similarly,  $u$  and  $v$ , being  $x$  and  $y$  velocities; have the form

$$u(x, y, t) = \Re \left[ \hat{u}_1(y) e^{j(kx - \omega t)} - \hat{u}_2(y) e^{j(kx + \omega t)} \right] \quad (9a)$$

$$v(x, y, t) = \Re \left[ \hat{v}_1(y) e^{j(kx - \omega t)} - \hat{v}_2(y) e^{j(kx + \omega t)} \right] \quad (9b)$$

where  $\Re$  denotes the real part of the complex form of primitive variables. Since the problem is linear, we can decompose the solution into two parts

$$u(x, y, t) = u_1(x, y, t) - u_2(x, y, t) \quad (10)$$

where

$$u_1(x, y, t) = \Re \left[ \hat{u}_1(y) e^{j(kx - \omega t)} \right] \quad (11a)$$

$$u_2(x, y, t) = \Re \left[ \hat{u}_2(y) e^{j(kx + \omega t)} \right] \quad (11b)$$

and similar relationships for  $p$  and  $v$  can be derived.

### 3.2. Solution method

Substituting the values of  $u_1$  and  $p_1$  in equation (7), we have

$$-j\omega \rho \hat{u}_1(y) = -jk \hat{p}_1 + \mu \frac{d^2 \hat{u}_1(y)}{dy^2} \quad (12)$$

rearranging variables and comparing it to the standard form gives

$$\frac{d^2\hat{u}_1(y)}{dy^2} + \alpha^2 \hat{u}_1(y) = Q \quad (13a)$$

$$\alpha^2 = \frac{j\omega\rho}{\mu} \quad (13b)$$

$$Q = \frac{jk\hat{p}_1}{\mu} \quad (13c)$$

Since these equations have a forcing term  $Q$  on the right, the solution is the sum of homogeneous and particular solutions. Homogeneous solution is given by

$$\hat{u}_{1h}(y) = A_1 \cos \alpha y + B_1 \sin \alpha y \quad (14)$$

We assume that the particular solution  $\hat{u}_{1p}$  will be a constant since the forcing function is a constant and hence the total solution is

$$\hat{u}_1(y) = \hat{u}_{1h}(y) + \hat{u}_{1p} \quad (15)$$

substituting the total solution back into the ODE given by equation (13a) we get

$$\hat{u}_{1p}(y) = \frac{k\hat{p}_1}{\omega\rho} \quad (16)$$

therefore the solution is

$$\hat{u}_1(y) = A_1 \cos \alpha y + B_1 \sin \alpha y + \frac{k\hat{p}_1}{\omega\rho} \quad (17)$$

boundary conditions are

$$\hat{u}_1(y) \Big|_{y=\pm H} = 0 \quad (18)$$

solving for  $A_1$  and  $B_1$ , we get

$$A_1 = -\frac{k\hat{p}_1}{\omega\rho \cos \alpha H} \quad (19a)$$

$$B_1 = 0 \quad (19b)$$

hence final solution is

$$\hat{u}_1(y) = \frac{k\hat{p}_1}{\omega\rho} \left[ 1 - \frac{\cos \alpha y}{\cos \alpha H} \right] \quad (20)$$

substitute this value into continuity equation (5a) to obtain

$$\frac{d\hat{v}_1(y)}{dy} = -jk\hat{u}_1(y) \quad (21)$$

integrate and get

$$\hat{v}_1(y) = \frac{jk^2 \hat{p}_1}{\omega \rho} \left[ \frac{\sin \alpha y}{\alpha \cos \alpha H} - y \right] + C_1 \quad (22)$$

where  $C_1$  is the integration constant. We have two variables to solve for, namely  $\hat{p}_1$  and  $C_1$  and two boundary conditions for  $\hat{v}_1$

$$\hat{v}_1|_{y=-H} = -\frac{j\omega A}{2} \quad (23a)$$

$$\hat{v}_2|_{y=+H} = \frac{j\omega A}{2} \quad (23b)$$

solving for the two variables, we get

$$C_1 = 0 \quad (24a)$$

$$\hat{p}_1 = \frac{A\rho\omega^2}{2k^2 \left( H - \frac{\tan \alpha H}{\alpha} \right)} \quad (24b)$$

substituting  $\hat{p}_1$  to solve for  $\hat{u}_1(y)$ , we get

$$\hat{u}_1(y) = \frac{\alpha A \omega (\cos \alpha H - \cos \alpha y)}{2k (\alpha H \cdot \cos \alpha H - \sin \alpha H)} \quad (25)$$

where  $\alpha = \sqrt{j\omega/\nu}$ ;  $\nu$  is the kinematic viscosity. Similarly we can solve for  $\hat{v}_1(y)$ .

Proceeding in the same way for  $\hat{u}_2(y)$  and solving the second part of the linear problem, we get

$$\hat{u}_2(y) = -\frac{\alpha A \omega (\cosh \alpha H - \cosh \alpha y)}{2k (\alpha H \cdot \cosh \alpha H - \sinh \alpha H)} \quad (26)$$

Therefore the total solution is given as

$$u(x, y, t) = \frac{\omega A}{2k} \Re \left[ \frac{\alpha (\cos \alpha H - \cos \alpha y)}{\alpha H \cdot \cos \alpha H - \sin \alpha H} e^{j(kx - \omega t)} \right. \\ \left. + \frac{\alpha (\cosh \alpha H - \cosh \alpha y)}{\alpha H \cdot \cosh \alpha H - \sinh \alpha H} e^{j(kx + \omega t)} \right] \quad (27)$$

Similarly, we can derive expressions for  $v(x, y, t)$  and  $p(x, y, t)$  as

$$v(x, y, t) = -\frac{\omega A}{2} \Re \left[ j \frac{y - \frac{\sin \alpha y}{\alpha \cos \alpha H}}{H - \frac{\sin \alpha H}{\alpha \cos \alpha H}} e^{j(kx - \omega t)} + j \frac{y - \frac{\sinh \alpha y}{\alpha \cosh \alpha H}}{H - \frac{\sinh \alpha H}{\alpha \cosh \alpha H}} e^{j(kx + \omega t)} \right] \quad (28)$$

$$p(x, y, t) = p_o - \frac{\omega^2 A \rho}{2k^2} \Re \left[ \frac{1}{H - \frac{\sin \alpha H}{\alpha \cos \alpha H}} e^{j(kx - \omega t)} + \frac{1}{H - \frac{\sinh \alpha H}{\alpha \cosh \alpha H}} e^{j(kx + \omega t)} \right] \quad (29)$$

#### 4. Results and discussion

A channel with dimensions  $L = 12\text{mm}$  and  $H = 150\text{ }\mu\text{m}$ , and actuating frequency  $f = 1\text{Hz}$  was studied. To avoid end effects on the solution, an entry and exit length of 20 hydraulic diameters was considered, which corresponds to 6mm of entry length. Pressure inlet boundary condition was applied on the two openings on either ends. These conditions are represented in Figure 3. A time dependent, first order implicit scheme was selected since it is unconditionally stable; however this scheme is lower in accuracy as compared to explicit schemes. Choosing the appropriate grid and time step resolutions circumvented this problem. The developed model was compared against simulations using a commercial CFD solver, FLUENT. For numerical simulations, three meshes of element size  $2 \times 10^{-5}$ ,  $3 \times 10^{-5}$  and  $4 \times 10^{-5}$  were chosen which are displayed in Figure 4; and results for  $x$ -velocity are compared at time  $t/T = 0.25$  at  $x/L = 0.25$  in Figure 5. It can be seen from Figure 5 that mesh size of the coarse mesh is suitable enough for the simulations, as there is no significant change in the velocity results. However, the graph also shows that the results are highly dependent on the chosen time step size--reducing the time step by half brings a change in the values by 50%. Therefore a time step size independence study was conducted until the computed variables showed no further change in their values.

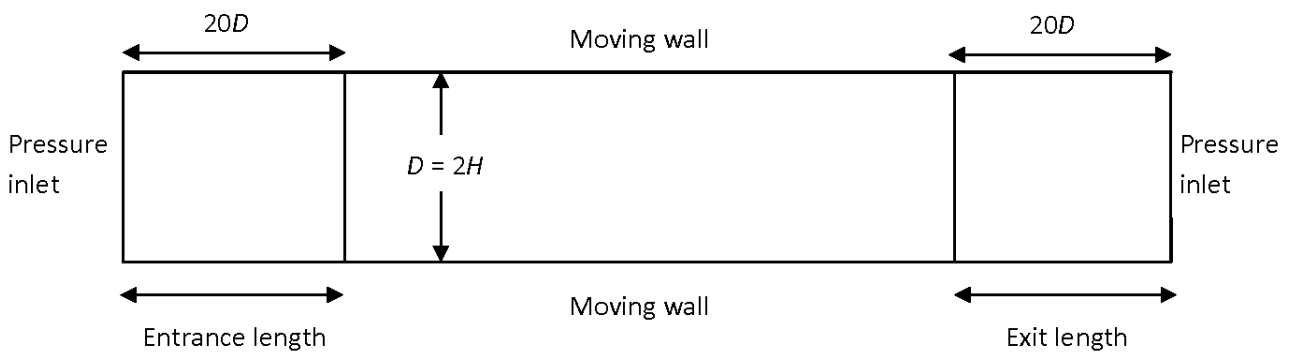


Figure 3. Boundary conditions for numerical computations. Drawing not to scale.

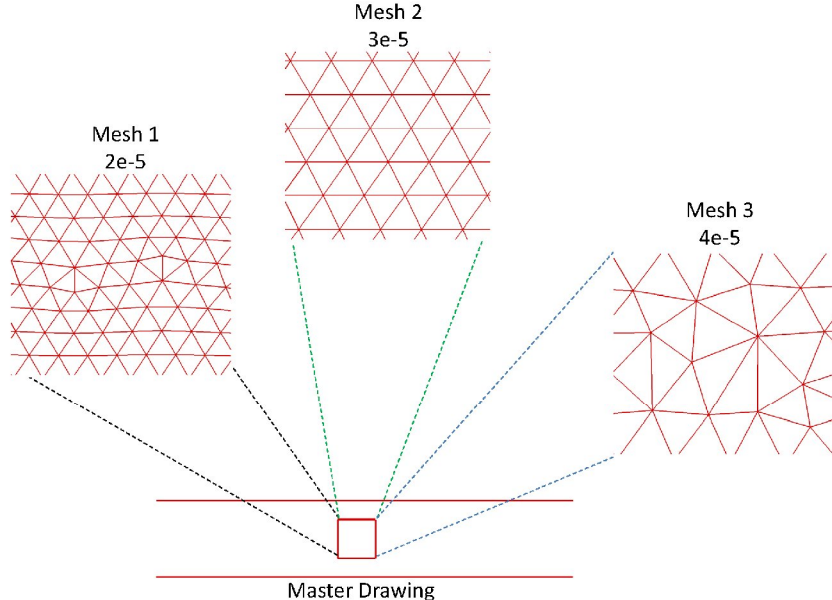
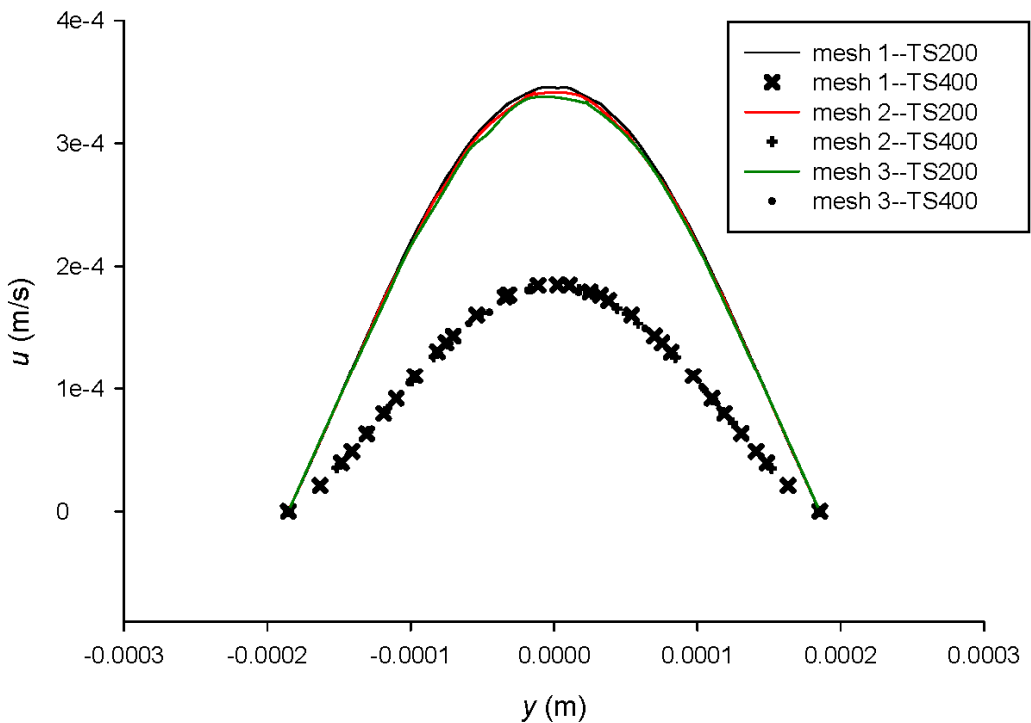


Figure 4. Meshes used for computations.


 Figure 5. Mesh independence test at  $t/T = 0.25$  and  $x/L = 0.25$ 

A mesh size of  $4 \times 10^{-5}$  was chosen and a time step size independence study was conducted until the numerical solution did not show any change with change in time step size. The final value of the time step size is of the order of  $10^{-6}$  with  $4 \times 10^5$  steps per cycle. At this resolution, the computed model over predicts analytical results by 18% as shown in Figure 6. This is quite reasonable because of the approximations involved while linearizing the Navier–Stokes equations. The velocity profile demonstrates the phenomenon of trapping with the presence of local recirculation zones. Figure 7 shows the velocity profile at  $x/L = 0.25$  and  $t/T = 0.5$ . At the same location and time instant,  $y$ -velocities are plotted in Figure 8, which confirm that analytical and numerical solutions are in good agreement.

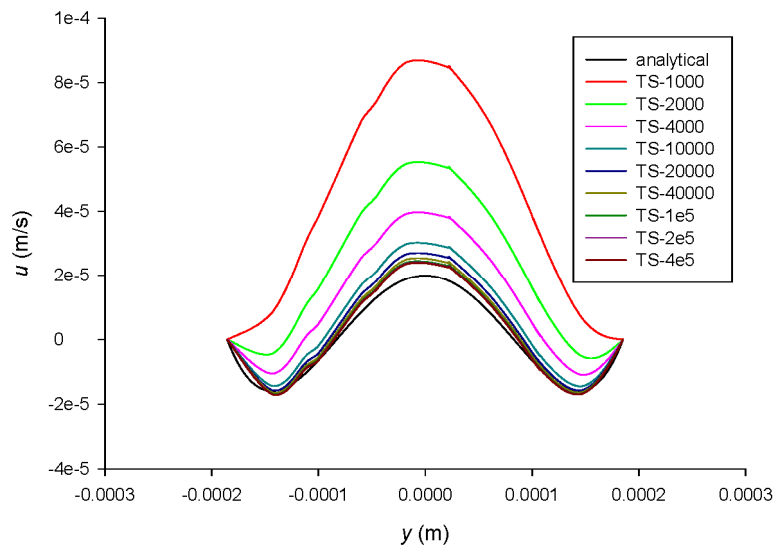


Figure 6. Time step independence test at  $t/T = 0.25$  and  $x/L = 0.25$

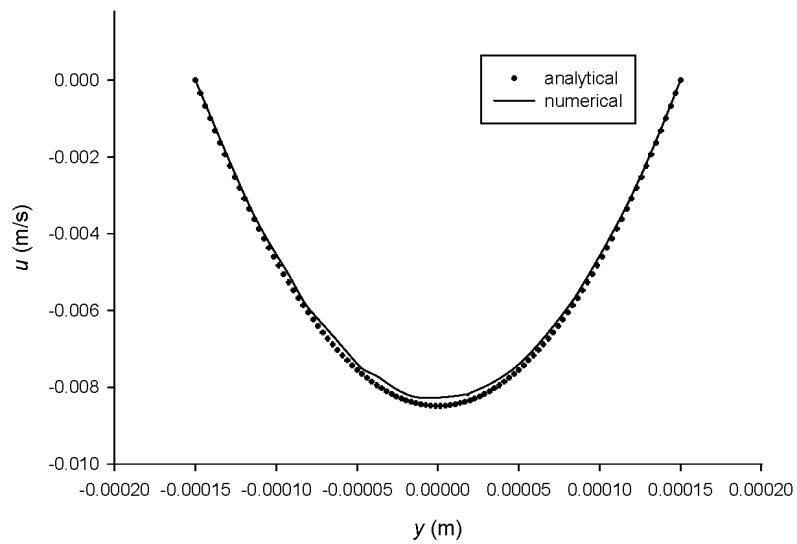


Figure 7. Streamwise velocity at  $t/T = 0.5$  and  $x/L = 0.25$

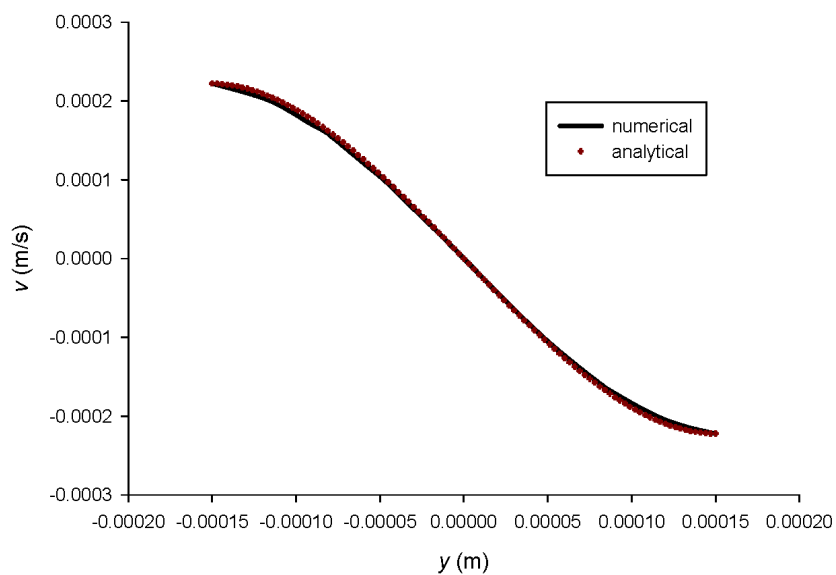


Figure 8. Normal velocity at  $t/T = 0.5$  and  $x/L = 0.25$

Figure 9 shows the centerline  $x$ -velocity across the length of the channel at  $t/T = 0.5$  and  $t/T = 1.0$ , where a comparison is made between computational and analytical results. A correct prediction of zero z-velocity at the center of the channel is observed. Contours of  $x$ -velocity at  $t/T = 0.25$  are shown in Figures 10(a) and 10(b) while Figures 11(a) and 11(b) show the same at  $t/T = 0.5$ . Excellent agreement between the two solutions is observed.

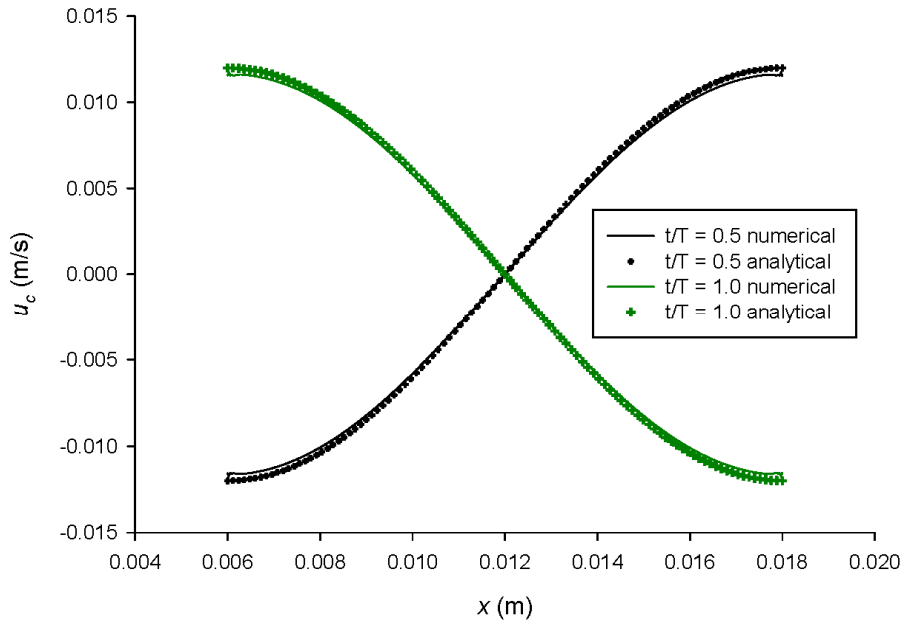


Figure 9. Centerline  $x$ -velocity at  $t/T = 0.5$  and  $t/T = 1.0$

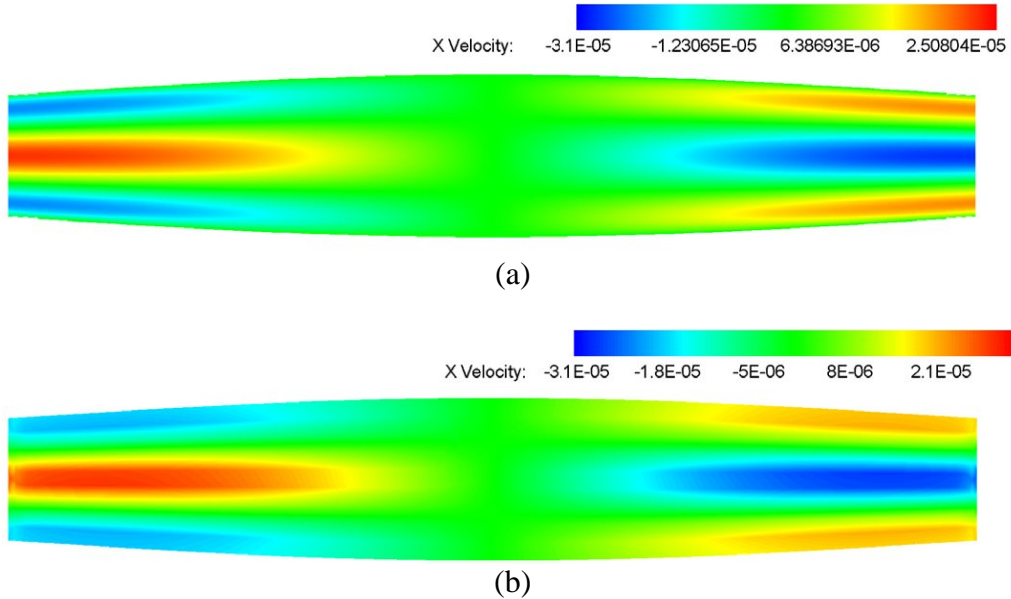


Figure 10. (a) Analytical and (b) numerical contours of  $x$ -velocity at  $t/T = 0.25$

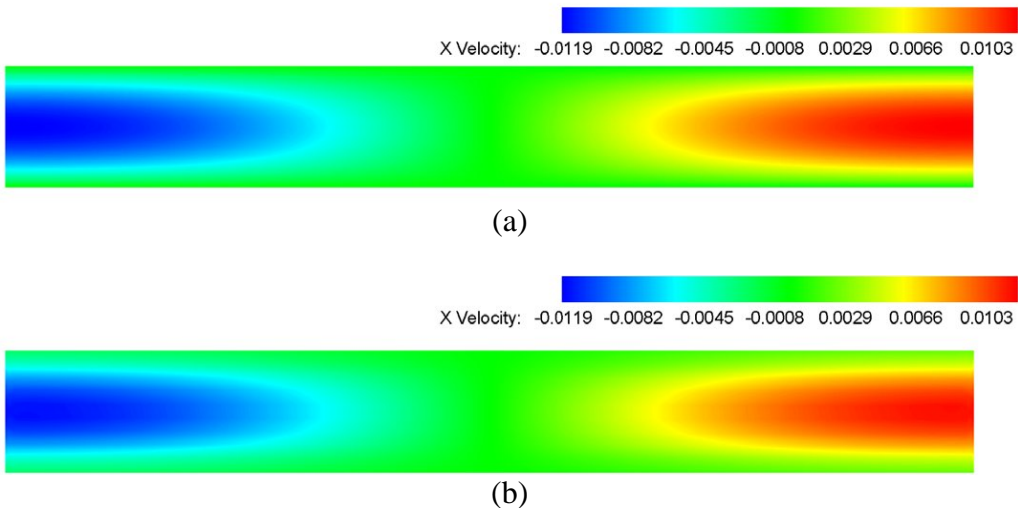


Figure 11. (a) Analytical and (b) numerical contours of  $x$ -velocity at  $t/T = 0.5$

## 5. Conclusions

A 2-D analytical model is developed for highly viscous flow between two deforming parallel plates. The deformation profile is decomposed into mode shapes using Fourier series approach, which are then used as a boundary condition. The governing Navier–Stokes equation is linearized by an order of magnitude analysis which helps in providing the solution of the flow field in a closed form. The results of pressure and velocities show a pulsatile nature. The results are then validated using CFD analysis, which shows a maximum difference of 18% in the  $x$ -velocity solution. The analytical model developed in this study may serve as an effective framework for understanding the nature and physics of flow field and making preliminary predictions. This framework can be used effectively for design and optimization of microdevices such as peristaltic micropumps, in which the flow physics operate in the same way. The generalized model can also be used to simulate and predict the performance of blood pumps in the context of biological flows.

## References

- [1] Stettler, J.C., P. Niederer, and M. Anliker, Theoretical analysis of arterial hemodynamics including the influence of bifurcations. Part I: mathematical models and prediction of normal pulse patterns. *Annals of Biomedical Engineering*, 1981. **9**(2): pp. 145–164.
- [2] Stettler, J.C., P. Niederer, M. Anliker, and M. Casty, Theoretical analysis of arterial hemodynamics including the influence of bifurcations. Part II: critical evaluation of theoretical model and comparison with noninvasive measurements of flow patterns in normal and pathological cases. *Annals of Biomedical Engineering*, 1981. **9**(2): pp. 165–175.
- [3] Sen, M., D. Wajerski, and M. Gad-el-Hak, A novel pump for MEMS applications. *Journal of Fluids Engineering—Transactions of the ASME*, 1996. **118**(3): pp. 624–627.
- [4] Burns, M., B. Johnson, S. Brahmasandra, K. Handique, J. Webster, M. Krishnan, T. Sammarco, P. Man, D. Jones, D. Heldsinger, C. Mastrangelo, and D. Burke, An integrated nanoliter DNA analysis device. *Science*, 1998. **282**(5388): pp. 484–487.
- [5] Selam, J.L., P. Micossi, F.L. Dunn, and D.M. Nathan, Clinical trial of programmable implantable insulin pump for type I diabetes. *Diabetes Care*, 1992. **15**(7): pp. 877–885.
- [6] Manton, M., Long-wavelength peristaltic pumping at low Reynolds-number. *Journal of Fluid Mechanics*, 1975. **68**(APR15): pp. 467–476.
- [7] Fung, Y. and C. Yih, Peristaltic transport. *Journal of Applied Mechanics*, 1968. **35**(4): pp. 669–675.

- [8] Shapiro, A., M. Jaffrin, and S. Weinburg, Peristaltic pumping with long wavelengths at low Reynolds number. *Journal of Fluid Mechanics*, 1969. **37**: pp. 799–825.
- [9] Ozawa, E., K. Bottom, X. Xiao, and R. Kamm, Numerical simulation of enhanced external counterpulsation. *Annals of Biomedical Engineering*, 2001. **29**(4): pp. 284–297.
- [10] Tatsumi, K., Y. Matsunaga, Y. Miwa, and K. Nakabe, Numerical study on fluid-flow characteristics of peristaltic pump. *Progress in Computational Fluid Dynamics*, 2009. **9**(3–5): pp. 176–182.
- [11] Tang, D. and M. Shen, Numerical and asymptotic solutions for the peristaltic transport of a heat-conducting fluid. *Acta Mechanica*, 1990. **83**(1–2): pp. 93–102.
- [12] Provost, A. and W. Schwarz, A theoretical-study of viscous effects in peristaltic pumping. *Journal of Fluid Mechanics*, 1994. **279**: pp. 177–195.
- [13] Li, M. and J. Brasseur, Non-steady peristaltic transport in finite-length tubes. *Journal of Fluid Mechanics*, 1993. **248**: pp. 129–151.
- [14] Natarajan, S. and M. Mokhtarzadeh-Dehghan, Numerical prediction of flow in a model of a (potential) soft acting peristaltic blood pump. *International Journal for Numerical Methods in Fluids*, 2000. **32**(6): pp. 711–724.
- [15] Bhadauria, R., Design and optimization of peristaltic micropumps using evolutionary algorithms, M.Sc. Thesis, Department of Mechanical Engineering. 2009, Virginia Commonwealth University: Richmond.
- [16] Bhadauria, R., R. Pidaparti, and M. Gad-el-Hak, Optimization of a peristaltic micropump with multiple moving actuators, in Submitted for publication. 2010.
- [17] Kreyszig, E., *Advanced Engineering Mathematics*. 1999: New York: Wiley.
- [18] Morgan, G. and J. Kiely, Wave propagation in a viscous liquid contained in a flexible tube. *The Journal of the Acoustical Society of America*, 1954. **26**(3): pp. 323–328.